IEEE Open Journal of the Communications Society

Received 7 May 2026; revised 18 May 2026; accepted 22 May 2026. Date of publication 26 May 2026; date of current version 19 June 2026.

Digital Object Identifier 10.1109/OJCOMS.2026.3696887

Broad-Band Nolen Beamforming Matrix Inspired by Groove Gap Waveguide Technology for Multi-Beam Antenna Arrays in mmWave Satellite-Oriented Space Multiplexing Systems

MOHAMMAD ALIBAKHSHIKENARI[1,2], BAL VIRDEE[3] (Senior Member, IEEE), YAZEED MOHAMMAD QASAYMEH[4], ALI ZIDOUR[5], MUHAMMAD AKMAL CHAUDHARY[6], CHAN HWANG SEE[7] (Senior Member, IEEE), PATRIZIA LIVRERI[8] (Senior Member, IEEE), NISAR AHMAD ABBASI[9], MOHAMADARIFF OTHMAN[10,11] (Member, IEEE), TAKFARINAS SABER[1], AND ERNESTO LIMITI[12] (Senior Member, IEEE)

[1]Lero, the Research Ireland Centre for Software, College of Science and Engineering, School of Computer Science, University of Galway, Galway H91 TK33, Ireland
[2]Department of Electrical and Electronics Engineering, Dogus University, Ümraniye, Istanbul 34775, Türkiye
[3]Center for Communications Technology, London Metropolitan University, London N7 8DB, U.K
[4]College of Engineering, Department of Electrical and Electronics Engineering, Majmaah University, Al Majma'ah 11952, Saudi Arabia
[5]Electrical Systems Engineering Department, University of M'hamed Bougara, Boumerdes 35000, Algeria
[6]Department of Electrical and Computer Engineering, Ajman University, Ajman, United Arab Emirates
[7]School of Computing, Engineering and the Built Environment, Edinburgh Napier University, Edinburgh EH10 5DT, U.K
[8]Department of Engineering, University of Palermo, Palermo 90128, Italy
[9]School of Systems Engineering, Department of Electrical Engineering, Bahrain Polytechnic, Isa Town 33349, Bahrain
[10]National Centre for Particle Physics, Universiti Malaya, Kuala Lumpur 50603, Malaysia
[11]Faculty of Engineering, Department of Electrical Engineering, Universiti Malaya, Kuala Lumpur 50603, Malaysia
[12]Electronics Engineering Department, University of Rome "Tor Vergata,", Rome 00133, Italy

CORRESPONDING AUTHOR: M. ALIBAKHSHIKENARI (mohammad.alibakhshikenari@universityofgalway.ie)

Co-funded by the European Union. Views and opinions expressed are however those of the author(s) only and do not necessarily reflect those of the European Union or the European Research Executive Agency. Neither the European Union nor the granting authority can be held responsible for them. Besides that, this publication has emanated from research jointly funded by Taighde Éireann–Research Ireland under Grant number 13/RC/2094_2, the European Union's Marie Sklodowska-Curie Actions under grant number 101126578 and was supported in part by University of Galway.

ABSTRACT This work presents the design and experimental validation of an integrated single-layer 4×4 Nolen beamforming matrix (NBM) implemented in groove gap waveguide (GGW) technology as an enabling front-end for multi-beam satellite gateway systems. The matrix is designed for operation within the 30–40 GHz upper Ka-band region, with optimal impedance matching and beamforming performance centered around 38 GHz, offering low-loss planar routing suitable for compact mmWave front-end architectures. The network combines broadband H-plane directional couplers (3.04, 4.77, and 6.0 dB) with fundamental and delay-compensation phase shifters to equalize amplitudes and maintain progressive phase. A WR-28-compatible input-feeding transition enables practical interfacing without disturbing the internal phase states, and a linear 4×4 slot-array antenna is integrated to demonstrate wide-angle multi-beam radiation. In contrast to prior Nolen matrices, including recent GGW implementations, this work introduces a fully single-layer GGW realization with parallel routing and built-in delay compensation, achieving phase error within ($\pm 10^\circ$), near-equalized amplitudes, and simplified fabrication within a compact footprint. In particular, compared to the recent GGW-based Nolen matrices, which employ the multilayer configurations and report only simulation results, the proposed work demonstrates the first experimentally validated single-layer GGW Nolen matrix with integrated feeding transition and radiating array. Measurements confirm return loss better than -15 dB, port-to-port isolation exceeding 15 dB, amplitude imbalance within ± 1.2 dB (around 6 dB nominal output), and phase error within $\pm 10^\circ$ with stable phase progression around 38 GHz.

INDEX TERMS Nolen beamforming matrix (NBM), groove gap waveguide (GGW), multi-beam antenna arrays, mmWave, space and satellite multiplexers.

I. INTRODUCTION

BEAMFORMING networks (BFNs) for multi-beam antennas are increasingly central to satellite communication systems because they enable directional transmission and reception, spatial selectivity, and interference mitigation [1], [2]. These capabilities improve link reliability, spatial selectivity, and interference mitigation and coverage in dense tag environments [3], [4]. By precisely controlling signal phase and amplitude, BFNs enhance link budgets, reduce collisions, and enable sectorized coverage in logistics, retail, and industrial space and satellite deployments [5], [6]. These strengths complement broader uses in terrestrial and space telecommunications [7], [8] and align with phased and beam-steered architectures envisioned for emerging 5G and 6G platforms [9]. The performance of any BFN depends on its topology, the radiating elements, and their spatial arrangement, which together determine the amplitude and phase profiles required for forming multiple, well-separated beams. BFNs are broadly categorized into digital and RF (analog) beamforming networks [10]. Digital BFNs are prevalent in adaptive arrays [11] but add complexity, power consumption, and cost that can be prohibitive for multi-beam space and satellite multiplexers.

RF beamforming networks (BFNs), which are widely used in fixed multi-beam arrays, are typically classified as either lens-based or circuit-based. Lens-based approaches, such as Luneburg [12], Ruze [13], and Rotman lenses [14], [15], provide true-time-delay characteristics and wideband performance; however, their large physical size, higher insertion loss, and packaging complexity can limit practical integration. In contrast, circuit-based BFNs—including Blass [16], Nolen [17], [18], and Butler matrices [19], [20]—offer more compact, low-loss solutions that are well suited for planar RF front-end implementations. The Butler matrix is widely deployed thanks to its symmetric and balanced paths, while the Nolen matrix has gained renewed attention for advantages particularly attractive in dense, high-frequency layouts such as elimination of line crossings, scalability in port count, and an inherently planar routing architecture.

A long-standing challenge of the traditional Nolen matrix is its limited bandwidth, arising from phase dispersion caused by unequal electrical path lengths. Unlike the inherently balanced Butler matrix, a conventional Nolen network struggles to preserve constant inter-port phase progression across frequency, which is problematic for wideband reader operation and for minimizing beam squint. This motivates enhanced Nolen topologies that retain architectural benefits while improving bandwidth and phase stability.

Recent work has begun exploring Nolen matrices in gap-waveguide (GW) technology. For example, Castro et al. [21] demonstrated a 4×4 GW-based Nolen matrix operating at 38 GHz; however, their design relies on a multilayer configuration and is limited to simulation results, without experimental validation or integration with a practical feeding network and radiating structure. The present work instead focuses on a groove gap waveguide (GGW) realization that is experimentally validated and implemented as a complete beamforming front-end. To improve performance, a predominantly parallel routing architecture is adopted together with integrated delay-compensation phase shifters, enabling enhanced phase stability and improved bandwidth behavior compared with [21].

In this context, the delay-compensation sections correspond to additional phase-shifting elements introduced along selected signal paths to correct phase imbalances caused by unequal electrical lengths and coupler-induced phase delays. By properly tailoring these compensations, the network maintains the required progressive phase relationship across output ports over a wide frequency range.

Several recent studies have explored Nolen matrix implementations at higher frequencies; however, many of these works remain limited to specific technologies or lack system-level validation. This highlights the need for experimentally verified mmWave beamforming networks that bridge the gap between theoretical designs and deployable systems.

Motivated by these developments, our earlier work presented at APMC 2025 [22] established general design guidelines for implementing mmWave beamforming matrices using GGW technology, demonstrating flexibility in realizing both Butler and Nolen configurations with arbitrary port counts. Building on these guidelines, the present work develops a free-crossover 4×4 Nolen beamforming matrix and extends the concept to a fully integrated system by incorporating a WR-28 compatible input feeding transition and a 4×4 slot-array antenna. The design is validated through comprehensive measurements. Consequently, this work advances the state of the art by providing a GGW-based Nolen matrix with improved phase accuracy, wideband operation, and complete system-level integration enabling wide-angle multi-beam radiation.

In this work, we present a single-layer 4×4 Nolen matrix implemented in GGW technology, an emerging platform for low-loss, high-isolation mmWave interconnects and passive components [23], [24], [25], [26], [27], [28]. The proposed design targets upper Ka-band operation (30–40 GHz) with optimum performance near 38 GHz, a regime relevant to exploratory mmWave high-resolution sensing. Operation in this upper Ka-band range is particularly attractive for emerging mmWave platforms because it aligns with several high-impact application domains. The 33–39 GHz region supports high-resolution sensing and multi-beam interrogation for industrial automation environments, enabling fine spatial selectivity and rapid sector scanning. It also overlaps with candidate FR2 extensions for 5G and early 6G testbeds, where compact multi-beam front ends are required for beam tracking and localized coverage. In the non-terrestrial domain, portions of the upper Ka-band are allocated for satellite feeder links, high-throughput gateway antennas, and electronically steered user terminals, all of which benefit from low-loss, multi-beam beamforming networks. These combined terrestrial and space-oriented use cases therefore motivate a compact, broadband Nolen matrix capable of delivering stable multi-beam performance across much of the 30–40 GHz region.

Given these motivations, a predominantly parallel physical layout is adopted to minimize routing imbalance, and delay-compensation sections are introduced to correct residual phase errors. The network employs broadband couplers together with fundamental and compensating phase shifters to equalize output amplitudes and enforce near-constant phase progression across the band.

To facilitate practical evaluation and real-world interfacing, we introduce an input feeding transition compatible with a WR-28 waveguide flange adapter, enabling accurate measurement without disturbing the intended phase relations. Finally, a broadband linear slot-array antenna is integrated at the matrix outputs to validate multi-beam radiation and wide-angle beam scanning. The resulting GGW-based Nolen beamforming network combines single-layer planar implementation with low-loss operation, stable phase performance, and high isolation, making it a strong candidate for advanced antenna arrays and mmWave multi-beam systems in satellite-oriented applications. Despite recent progress, existing mmWave Nolen matrix implementations remain constrained by limited bandwidth due to phase dispersion, reliance on multilayer or complex structures, and a lack of experimentally validated system-level realizations. In particular, achieving stable phase progression across a wide frequency range while ensuring a practical and manufacturable design remains a significant challenge.

The present work addresses these limitations by combining a GGW-based implementation with an integrated delay-compensation strategy tailored for mmWave operation. Rather than focusing solely on footprint reduction, the proposed approach emphasizes low-loss propagation, high isolation, and stable phase performance at 38 GHz. The delay-compensation technique is co-designed with the GGW structure and implemented within a predominantly parallel routing architecture, enabling improved phase stability without increasing structural complexity. In addition, the design is experimentally validated as a complete beamforming front-end, including a practical input feeding transition and an integrated slot-array antenna.

A key contribution of this work is the first experimentally validated single-layer GGW Nolen matrix operating at 38 GHz in the upper Ka-band, which extends beyond the frequency range of most previously reported planar implementations.

The main contributions of this work can be summarized as follows:

1. A single-layer GGW-based 4 × 4 Nolen matrix with integrated delay-compensation strategy;
2. Experimental validation of phase-stable multi-beam operation at mmWave frequencies;
3. Integration of a WR-28 feeding transition and slot-array antenna into a complete beamforming system.

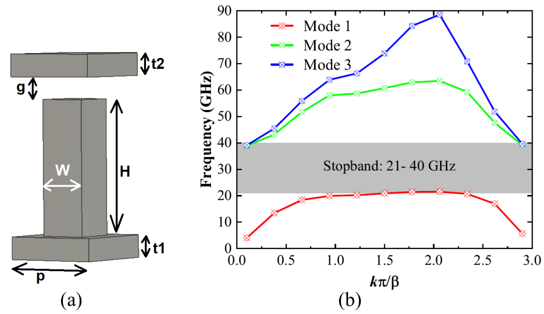

FIGURE 1. **(a) Structure of the proposed unit-cell configuration based on GW technology, and (b) its dispersion diagram.**

TABLE 1. **Pin's structural parameters.**

Parameter	Size (mm)
Height (*H*)	3
Width or diameter (*W*)	1
Periodicity (*p*)	2
Air gap (*g*)	0.5
Thickness of top and bottom layers (*t1*=*t2*)	0.5

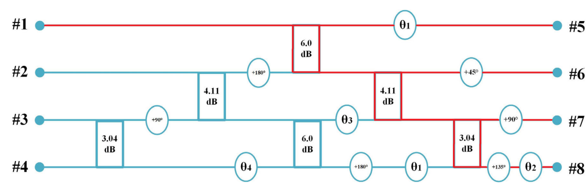

FIGURE 2. **Graphical representation of the proposed 4 × 4 NBM. The phase shift angle values of the compensator phase shifters are: $\theta_1=-37^{\circ}$, $\theta_2=-84^{\circ}$, $\theta_3=-90^{\circ}$, and $\theta_4=-116^{\circ}$.**

II. SINGLE LAYER NBM USING GGW TECHNOLOGY

A. UNIT-CELL DESIGN

As explained in [23], [24], and [25], Artificial Magnetic Conductor (AMC) layouts are crucial for GW structure implementations, providing band-stop behavior across the desired working frequencies. This part elaborates the proposed approach for designing the AMC structure for feasible GW implementation. The AMC structure is achieved using mushroom-like pins, one of the earliest and most used designs in GW structures [29]. In this case, the AMC structure is realized with fully metallic pins, a low-loss technique. These metallic pins can take various configurations, including rectangular cuboids [23], cylinders [30], cone-shaped forms [31], and even spring-like models [32].

It's important to note that while the geometric shape of the AMC pins has minimal impact on the working bandwidth [30], the choice of geometry often depends on manufacturing considerations. Several factors influence the bandwidth performance of this pin-based structure, such as the pin's width or diameter, height, the periodicity of the pin array, and the air gap between the pins and the top metallic surface. Fig. 1(a) demonstrates the topology of the proposed metallic pin with a rectangular cuboid shape, and its dispersion diagram shown in Fig. 1(b) demonstrates a broad stopband between 21–40 GHz. The structural parameters are listed in Table 1.

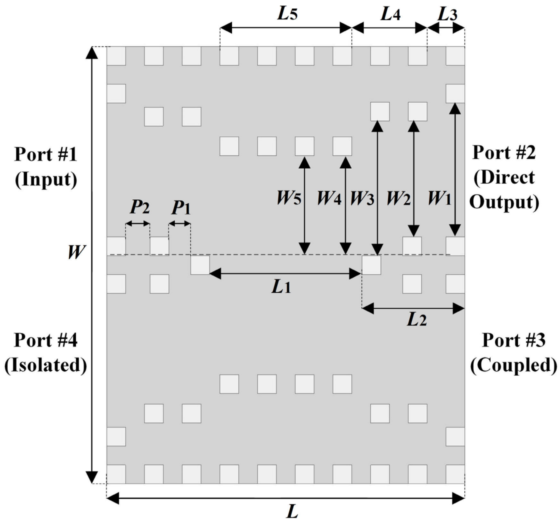

FIGURE 3. H-plane directional coupler using GGW technology.

TABLE 2. Coupler's structural parameters.

Parameters (mm)	3.04 dB	4.77 dB	6.0 dB
L	19	19	19
L_1	8.1	9	9
L_2	5.45	5	5
L_3	2	4	4
L_4	4	4	4
L_5	7	3	3
W	23.224	23.224	23.224
W_1	7.112	7.112	7.112
W_2	5.892	7.112	7.112
W_3	6.892	6.906	6.906
W_4	5.312	6.056	6.906
W_5	5.312	5.212	5.212
P_1	1.150	1	1
P_2	1.300	1	1

B. CIRCUIT-BASED BUILDING BLOCK OF THE NBM

The proposed 4×4 NBM layout includes H-plane directional couplers with attenuation values of 3.04, 4.77, and 6.0-dB, each providing a 90° phase difference between their coupled and direct ports. It also incorporates phase shifters with phase differences of 45°, 90°, 135°, and 180°, as illustrated in Fig. 2. To achieve wideband design capability, the components of the NBM are arranged in a 'parallel' layout. Additionally, to optimize performance, delay compensation phase shifters have been designed and integrated into the beamforming network.

1) COUPLER DESIGN

Fig. 3 illustrates the topology of the GGW directional couplers with matched H-plane impedance steps, which prevent the propagation of the unwanted TE30 mode [33]. The three different couplers are optimized using the 3-D electromagnetic simulation tool CST Microwave Studio. Table 2 represents the geometric parameters.

The apparent gap between the first and second row of pins in the coupler is intentional. This clearance forms the coupling region between the two GGW channels and is required to achieve the target coupling levels. Although the surrounding AMC "bed-of-nails" structure appears locally sparse, the stopband characteristic of the GGW pin lattice remains intact over 30–40 GHz, ensuring that fields are laterally confined and preventing unintended leakage. This is supported by the simulated S-parameters, which show return loss and isolation better than 15 dB across the band, indicating negligible parasitic radiation. Additional parametric studies showed that partially filling this region with pins increases confinement only marginally but disrupts the coupling aperture, leading to deviations from the desired 3.04-, 4.77-, and 6.0-dB coupling responses and a reduction in broadband matching. For this reason, the final pin configuration maintains a deliberate clearance around the coupling window while preserving the required GGW stopband behavior and wideband coupler performance.

Fig. 4 presents the S-parameter results for the directional couplers over a broadband frequency range of 30–40 GHz. For the 3.04 dB coupler, the coupling value ranges from 2.44 dB at 30 GHz to 3.97 dB at 40 GHz, with a nominal value of 3.04 dB at the target frequency of 38 GHz. For the 4.77 dB coupler, the coupling value varies from 3.60 dB between 32 and 33 GHz to 6.65 dB at 40 GHz, with a nominal value of 4.77 dB at 38 GHz. Finally, for the 6.0 dB coupler, the coupling coefficient ranges from 3.60 dB between 35 and 36 GHz to 9.82 dB at 40 GHz, with a nominal value of 6.0 dB at 38 GHz. For all three couplers, return losses and isolations are greater than 15 dB, and the phase shift between the direct output and coupled ports is consistently 90°, i.e., Ang. S_{21}–Ang. S_{31} = 90° across the entire 30–40 GHz with the optimal results observed near 38 GHz.

The use of different coupling values, i.e. 3.04 dB, 4.77 dB, and 6.0 dB, is essential to achieve the required power distribution at the output ports of the NBM. In a 4×4 NBM topology, each input signal passes through a unique sequence of couplers before reaching the outputs. The differing coupling strengths are therefore synthesized to ensure equal output amplitudes (ideally 6.02 dB) for all ports while preserving the required 90° phase difference between the direct and coupled ports, regardless of the number of stages traversed. This tailored approach ensures power balance and avoids the need for attenuators or terminations, contributing to a more integrated and efficient design.

2) PHASE-SHIFTER DESIGN

Four fundamental phase shifters with values of 45°, 90°, 135°, and 180° are designed by combining the characteristics of unequal-length ($L \neq L_1$) and unequal-width ($W_1 \neq W_2$) transmission lines, except for the 45° phase shifter that has $L = L_1$. They have been arranged as shown in Fig. 2. The topology of these fundamental phase shifters, along with their structural parameters, is depicted in Fig. 5 and detailed in Table 3. As indicated, the most critical geometric parameters for realizing the fundamental phase shifters are L_1, L_2, and W_2.

Fig. 6 shows the reflection coefficients of the phase shifters, which are below -15 dB across the 30–40 GHz. All phase shifters achieve required phase shifts at 38 GHz.

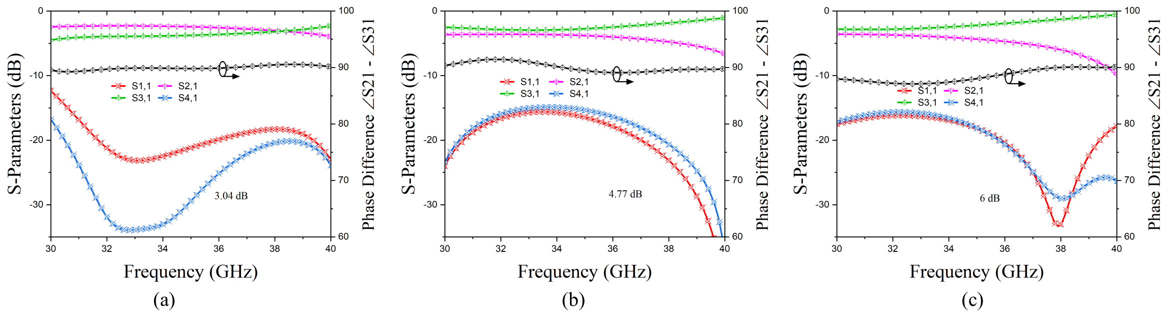

FIGURE 4. Couplers' S-parameters include the reflection coefficients (S_{11} < -10 dB), transmission coefficients (S_{21} and S_{31}), isolation (S_{41}), and the phase-shift difference between the direct output and coupled ports. (a) 3.04-, (b) 4.77-, and (c) 6.0-dB.

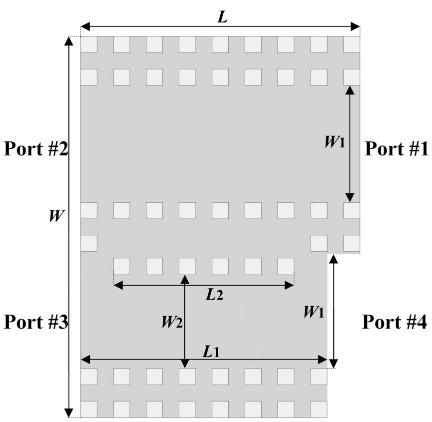

FIGURE 5. Unequal-width unequal-length phase shifters.

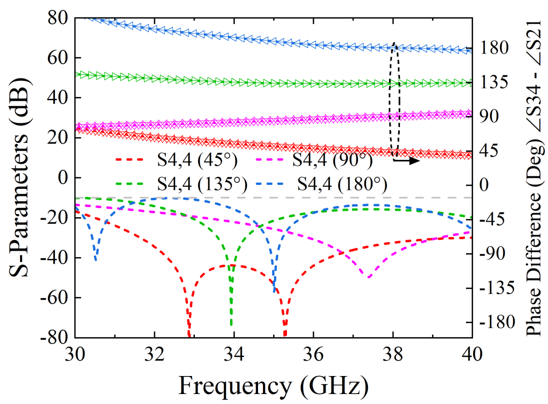

FIGURE 6. Characteristics of 45°, 90°, 135°, & 180° phase shifters.

TABLE 3. Phase-shifter's structural parameters.

Parameters (mm)	L	L_1	L_2	W	W_1	W_2
Fundamental Phase Shifters						
45°	15	15	11	23.224	7.112	5.492
90°	11	9	3	23.224	7.112	6.012
135°	17	15	11	23.224	7.112	5.712
180°	23	21	17	23.224	7.112	5.512
Couplers' Delay Compensation Phase Shifters						
−37°	11	9	-	23.224	7.112	11.112
−84°	21	19	-	23.224	7.112	11.112
−90°	23	21	-	23.224	7.112	11.112
−116°	29	27	-	23.224	7.112	11.112
Combination of Consecutive Phase Shifters						
135°−84° = 51°	15	15	11	23.224	7.112	5.392
180°−37° = 143°	17	15	11	23.224	7.112	5.582

3) COUPLER'S DELAY COMPENSATION

In a conventional Nolen matrix, signals propagating from a given input port to different output ports experience unequal electrical path lengths due to the sequential arrangement of couplers and phase shifters. These path-length differences introduce frequency-dependent phase errors, which degrade beamforming accuracy and limit bandwidth. To mitigate this effect, dedicated delay-compensation sections are introduced in the proposed design. These sections consist of additional phase shifters strategically placed along specific signal paths to counteract the excess phase delay accumulated in longer routes and the insertion phase of the directional couplers.

TABLE 4. The path length differences and the corresponding phase compensations of the proposed parallel physical layout.

Output Port	Relative Path Length Difference (mm)	Required Phase Compensation (°)
Port 1	0.81	–37°
Port 2	1.84	–84°
Port 3	2.67	–90°
Port 4	3.57	–116°

Fig. 2 highlights the different routes between input port 1 and the output ports 5–8. The signal propagated toward ports 7 and 8 goes via the 6.0-, 4.77-, and 3.04-dB couplers sequentially. The signal propagated toward port 6 goes via the 6.0- and 4.77-dB couplers. To achieve wideband operation, the insertion phase of the 3.04-dB coupler's direct ports should be compensated for signals going to ports 5 & 6. Additionally, the electrical way between ports 1 & 5 needs to compensate the phase-delay to account for the insertion phase generated by the 4.77-dB coupler's direct port, along with the delay from the 3.04-dB coupler.

Further phase shifts are necessary for sufficient broadband operation of other input ports, as demonstrated in Fig. 2. These phase shifts are additional to those typically needed by a standard NBM, with numerical amounts shown in the figure. The layout of the couplers' delay compensation

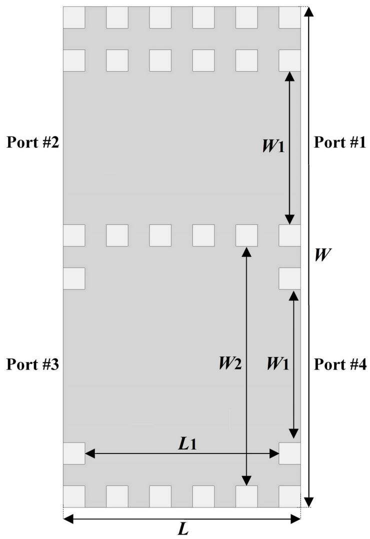

FIGURE 7. Structure of the coupler's delay compensation phase shifters for phase shift angles of –37° – 84° – 90° and –116°.

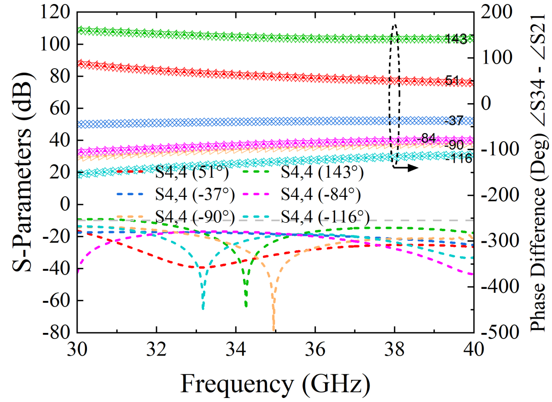

FIGURE 8. Characteristics of the coupler's delay compensators.

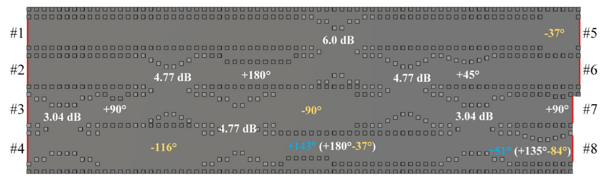

FIGURE 9. Proposed 4 × 4 NBM using GGW technology.

phase shifters of the proposed parallel physical layout, along with their structural parameters and the path length differences are displayed in Fig. 7 and summarized in Tables 3 and 4. As noted in Table 3, instead of using two consecutive phase shifters, their combined values are utilized in the final matrix structure. Specifically, a −84° delay compensation phase shifter is combined with a 135° fundamental phase shifter, resulting in a single-phase shifter of 51°. Similarly, on the path between ports 4 and 8, a −37° delay compensation phase shifter in series with a 180° fundamental phase shifter results in a combined phase shifter of 143°. This combination simplifies the matrix layout.

The required compensation values are determined based on the relative path-length differences between signal routes, as summarized in Table 4. These differences are translated into equivalent phase shifts at the design frequency (38 GHz), and corresponding GGW phase shifters are designed to realize the required corrections. To minimize layout complexity, compensation phase shifters are combined with adjacent fundamental phase shifters wherever possible, resulting in a reduced number of physical components while preserving the desired phase response.

Fig. 8 shows the reflection coefficients and differential phase shifts for the coupler's delay compensation phase shifters for phase shift angle of −37°, −84°, −90°, and −116°, as well as the combined phase shifters of 51° and 143°. These phase shifters provide the required differential phase shifts at the desired frequency of 38 GHz, with reflection coefficients below −15 dB across 30–40 GHz.

Without compensation, the unequal electrical path lengths would lead to significant phase dispersion across the operating band. The introduced delay-compensation sections effectively reduce these deviations, resulting in a near-uniform phase progression with an error limited to approximately ±10° across the band.

C. IMPLEMENTATION BY COMPONENTS INTEGRATION

To implement the proposed 4 × 4 NBM, the H-plane directional couplers and phase shifters designed in the previous sections must be integrated. The configuration of this beamforming matrix is illustrated in Fig. 9. To construct a planar eight-port Nolen matrix, six H-plane directional couplers are combined with eleven phase shifters—six fundamental phase shifters and five coupler delay compensation phase shifters.

As previously mentioned, to simplify the design and decrease the number of phase shifters in the final Nolen matrix structure, the cascaded phase shifters shown in Fig. 2 (comprising both fundamental and coupler's delay compensation phase shifters) are merged by appropriately adding the relevant parameters, namely L_1, L_2, and W_2. Consequently, Fig. 9 shows nine phase shifters because the −84° phase compensator, which is in series with the 135° phase shifter located just before output port 8, has been combined into a single-phase shift of 51°. Additionally, a −37° phase compensator in series with the 180° phase shifter on the path between ports 4 & 8 is also combined, resulting in a phase shift of 143°, which has been incorporated in place of the original components. This integration of delay-compensation sections within the signal paths ensures that all output ports maintain a near-uniform phase progression across the operating band, which is critical for achieving broadband multi-beam performance.

Fig. 10 shows the S-parameters for input ports 1–4. The transmission coefficients exhibit some frequency-dependent variation, which is typical for wideband designs using GGW couplers and phase shifters. Despite this, power distribution remains within ±1.2 dB, which is acceptable for broadband beamforming. In addition, the port-to-port isolation remains

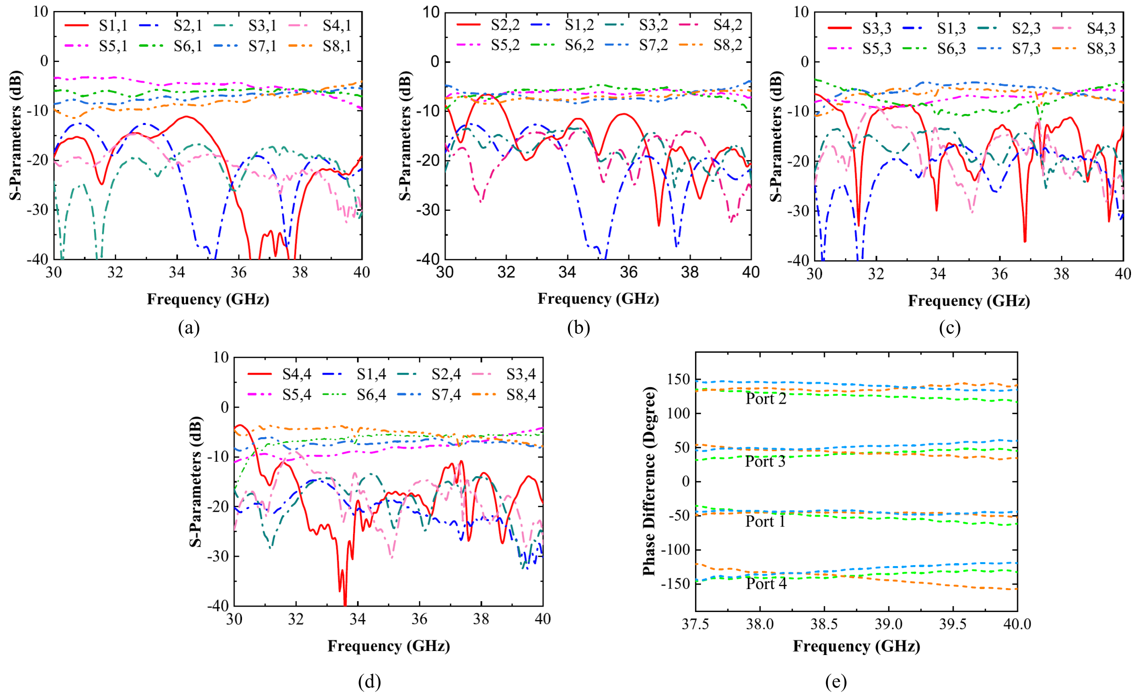

FIGURE 10. **S-parameters of the proposed 4 × 4 NBM, (a) Port 1, (b) Port 2, (c) Port 3, and (d) Port 4. To avoid crowding the curves, the isolations have been plotted only for port 1 because the other ports have a similar isolation response. (e) Phase differences between consecutive outputs.**

better than 15 dB across the operating band, confirming effective suppression of undesired coupling between channels.

It is noted that the transmission coefficients do not remain fully constant across the entire 30–40 GHz band. This behavior is expected in wideband implementations of the Nolen matrix, particularly when realized using practical GGW couplers and phase-shifting structures. Each H-plane coupler exhibits a frequency-dependent coupling response, as shown in Fig. 4, and the phase shifters likewise introduce slight dispersion over the band. When these components are cascaded within the serial architecture of the Nolen matrix, small variations accumulate and manifest as the measured amplitude ripples in the transmission responses. Such behavior has also been reported in previously published Nolen matrices across microstrip, SIW, and gap-waveguide technologies. Despite these inherent wideband challenges, the proposed design maintains amplitude imbalance within ±1.2 dB, and return loss and isolation better than 15 dB, confirming that the observed variations do not compromise the wideband beamforming capability of the system. At the target operating frequency of 38 GHz, the transmission coefficients are well equalized at approximately 6.2 dB for all input ports, closely aligning with the theoretically predicted value of 6.02 dB for a standard Nolen matrix.

Unlike the standard Nolen matrix, the insertion losses in this wideband design are consistent across different ports. In other words, the losses do not vary with the electrical path length; the shorter path (from port 1 to port 5) has nearly the same losses as the longer path (from port 4 to port 8). This uniformity is achieved because, in the proposed design, the signal path from port 1 to port 5 or port 8 is effectively the same, thanks to compensation. The same applies to signals from any other input ports to output ports, resulting in wideband performance across all paths.

Fig. 10(e) exhibits the phase dispersions between the output ports of the GGW-assisted NBM when each input port is excited. In a standard Nolen matrix, when an input port is stimulated, the phase differences between each pair of consecutive output ports should be equal. The average phase differences between the output ports of the proposed matrix at 38 GHz are −44.5°, +139.2°, +47.3°, and −136.7° when ports 1 through 4 are stimulated, respectively. This indicates an excellent agreement between the results of the proposed Nolen matrix and the theoretical results of a standard Nolen matrix (−45°, +135°, +45°, and −135°).

The results also demonstrate that the proposed matrix provides an almost constant phase dispersion amongst the whole frequency band of 30–40 GHz for all input ports. However, slight phase-progression deviations within ±10° are observed, that is partly because of the frequency-dependent specifications of the phase shifters. In other words, the serial feeding characteristic of a Nolen matrix contributes to the frequency-dependent phase. The incremental phase shift between neighbour outputs changes with frequency, yet despite this, the achieved results remain in good agreement across the entire bandwidth with a worst-case error of ±10°. This demonstrates the effectiveness of the proposed delay-compensation strategy, as the uncompensated structure would exhibit substantially larger phase deviations and degraded beamforming performance.

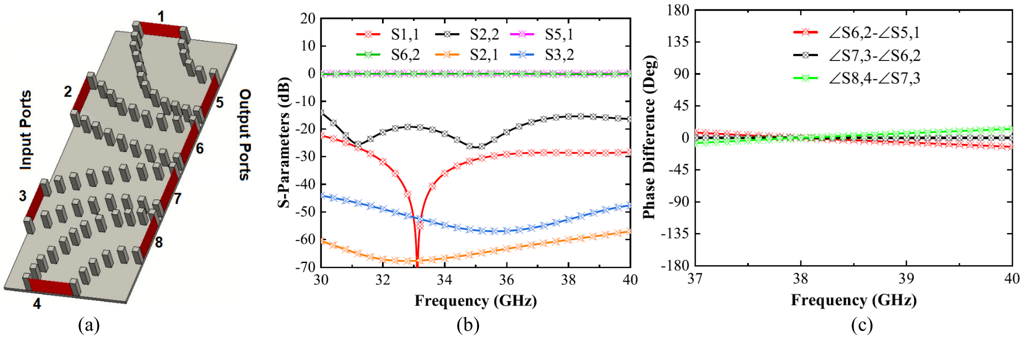

FIGURE 11. (a) Layout of the proposed IFT, (b) reflection coefficients, isolation, and transition coefficients between the input ports and their corresponding direct output ports, and (c) differential phase differences between the consecutive output ports at 38 GHz.

D. DESIGN OF INPUT FEEDING TRANSITION (IFT) AND ITS INTEGRATION TO NBM

For the experimental testing of the proposed NBM, it is essential to implement a feeding transition at the input ports to accommodate the WR28 waveguide flange adapters for proper excitation of the input ports. The operating frequency band of the matrix and the width of its waveguides (7.112 mm) are aligned with the frequency spectrum and the geometrical parameters of the WR28, that is why this waveguide flange adapter is chosen.

It is important to note that the performance of the IFT should not interfere with the matrix's overall performance. Specifically, the magnitude of the transmission coefficients between the input ports and their corresponding direct output ports should be approximately zero, i.e., $S_{51} = S_{62} = S_{73} = S_{84} \cong 0$ dB. Additionally, the phase differences between each pair of consecutive output ports should also be zero, meaning that the outputs should have the same phases at 38 GHz, i.e., Ang. S_{51} = Ang. S_{62} = Ang. S_{73} = Ang. S_{84}, ensuring that Ang. S_{62}–Ang. $S_{51} = 0°$. When these conditions are met, all signals passing through the IFT will enter the matrix with the same phase, ensuring that the IFT does not affect the matrix's phase performance. In this case, the IFT serves solely as a signal transition board.

The layout of the implemented IFT, which has a length of 21 mm and a width of 55.5 mm, along with its performance parameters are shown in Fig. 11. It is evident that the isolation between the input ports is sufficiently high. Due to the symmetry between ports 1 & 4 and ports 2 & 3, the isolation between ports 1 & 2 and ports 2 & 3 is ensured to prevent any repetition.

The next step in the design process is to integrate the designed IFT with the NBM to assess its impact on the matrix's performance. Fig. 12 represents the topology and performance parameters of the integrated NBM and IFT. It is evident that the matrix with the IFT exhibits almost identical performance to the matrix without the IFT, as shown in Fig. 10. This demonstrates the precision and effectiveness of the proposed IFT design.

It should be noted that, while the standalone IFT exhibits near-zero phase difference as shown in Fig. 11, small deviations are observed after integration with the Nolen matrix in Fig. 12(f). This is due to cascading effects, minor impedance mismatches, and fabrication tolerances, which introduce slight phase perturbations. However, these deviations remain negligible and do not impact the overall beamforming performance.

TABLE 5. Antenna's structural parameters.

Parameters	Size (mm)
L	49
W	13.112
H (height of pin)	3
t1 (thickness of the bottom layer)	0.5
t2 (thickness of the top layer)	0.5
Ls	6.13
S	1
g	1
L1	3
L2	1
w1	3.482
w2	3.5

E. SLOT ARRAY ANTENNA DESIGN

This section demonstrates the design and implementation of a slot array antenna for integration into the output ports of the matrix for the radiation process. First a single slot array antenna using GGW technology is developed to cover 30–40 GHz, as exhibited in Fig. 13. The antenna design includes a 0.5mm air gap between top and base layers, consistent with GGW principles. Antenna's geometrical parameters are listed in Table 5.

The layout of the 4×4 linear slot array antenna is displayed in Fig. 13. It shares the same structural parameters as the single slot array antenna but contains of four single slot array antennas arranged linearly. Fig. 13(b) demonstrates that each port covers the frequency range of 30–40 GHz with a reflection coefficient better than -15 dB, and the isolation between ports is better than 40 dB. Due to the symmetrical design of the array, ports 1 & 4, as well as ports 2 & 3, exhibit identical S-parameter performances.

The Cartesian and polar radiation patterns for ports 1 & 2 in both the H- and E-planes at 38 GHz are depicted in Figs. 13(c) and (d), respectively. These

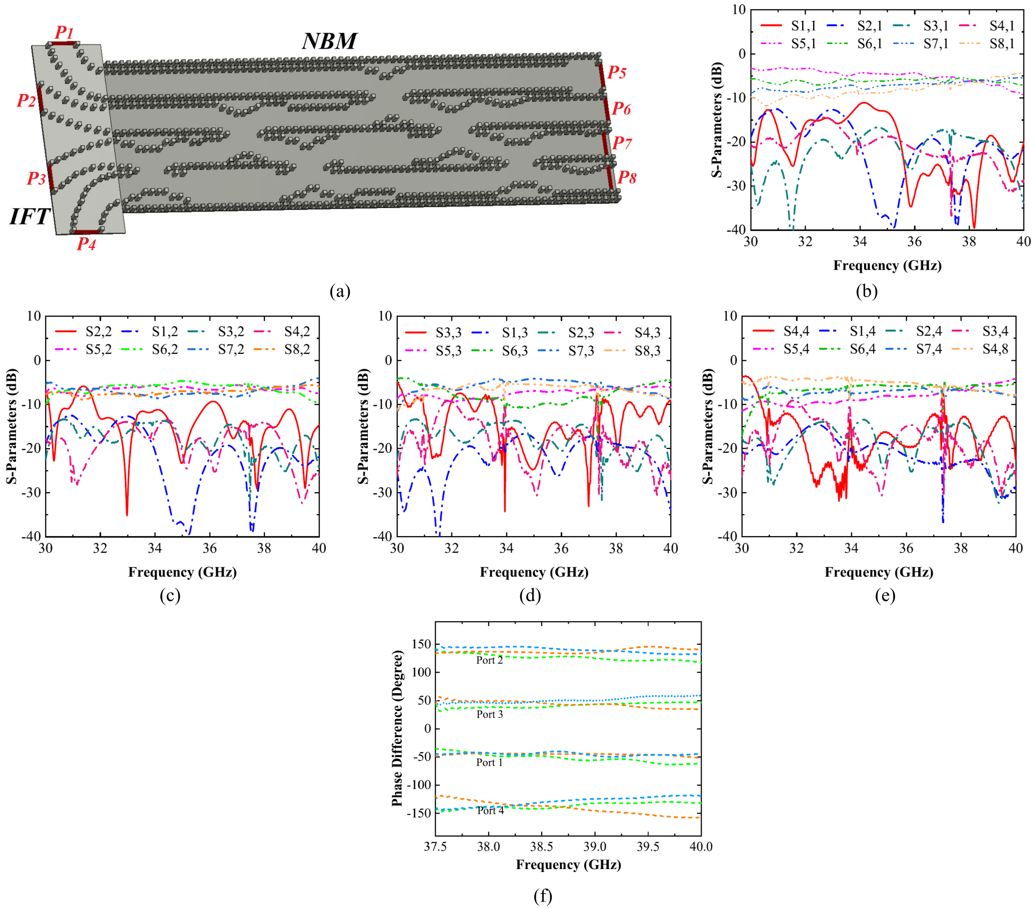

FIGURE 12. **(a) Topology of the integrated NBM and IFT, (b–e) reflection coefficients, isolation between input ports, and transition coefficients between the input ports and their corresponding direct output ports, (f) differential phase differences between the consecutive output ports.**

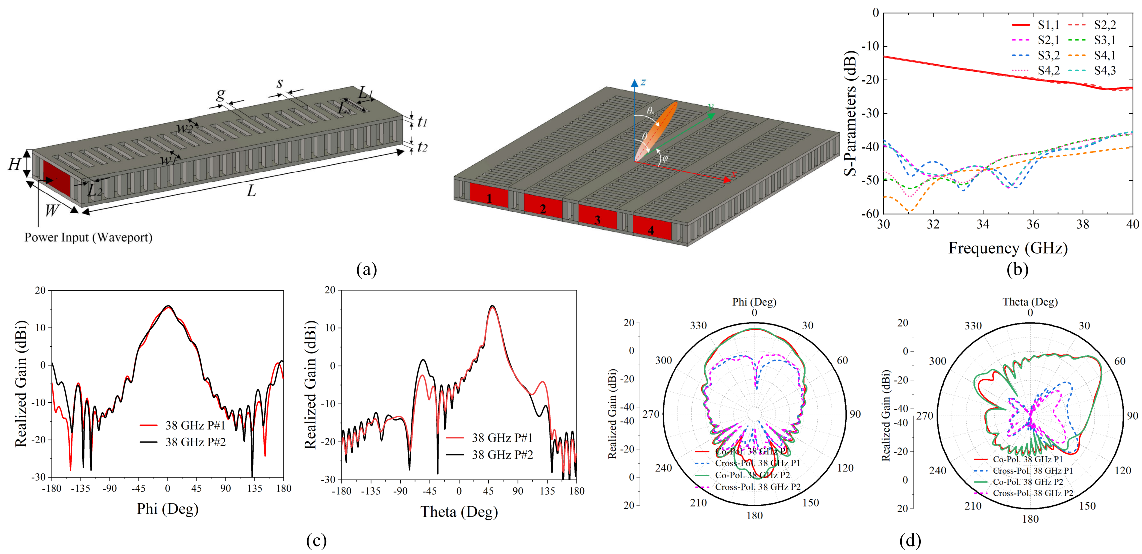

FIGURE 13. **(a) Layout of the single and 4 × 4 linear slot array antennas, (b) reflection coefficient, and (c) cartesian and (d) polar H-plane (left-side) and E-plane (right-side) radiation patterns of the 4 × 4 linear slot array antennas at 38 GHz.**

patterns indicate that the array antenna provides high radiation gains, exceeding 15 dBi, in both planes at 38 GHz.

F. ASSEMBLING

The final beamforming structure consists of the NBM, IFT, and a 4 × 4 linear slot array antenna, enabling the proposed

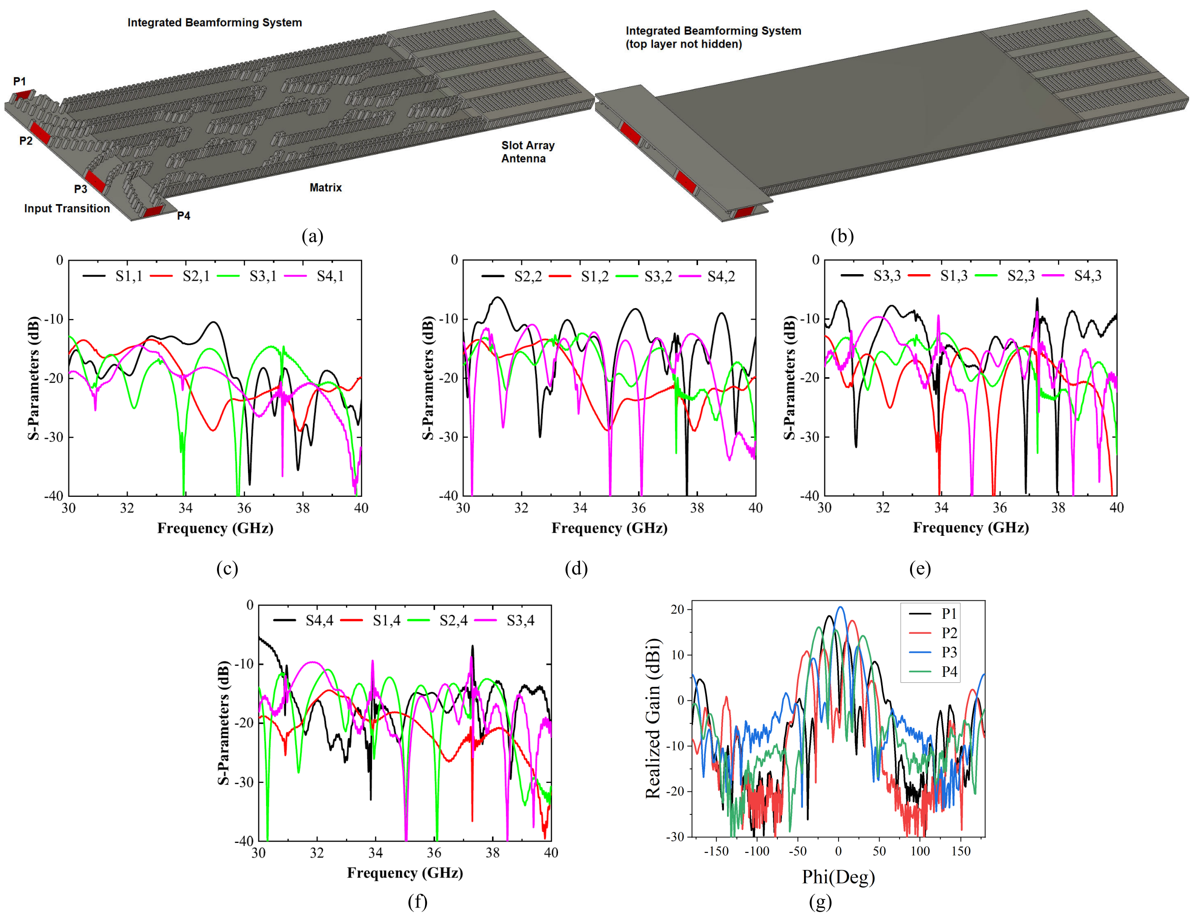

FIGURE 14. Proposed GGW-based beamforming network composed by NBM, IFT, and slot array antennas, (a) layout without top-layer, (b) layout with top-layer, (c–f) reflection coefficients (S_{11} <-10 dB) and isolation between the input ports, and (g) radiation patterns at 38 GHz.

system to radiate at various angles with wideband scanning capabilities at the target frequency of 38 GHz. The configuration is shown in Fig. 14. In Fig. 14(a), the top layer of the matrix and its IFT are hidden to provide a comprehensive view of the internal configuration and arrangement of sub-components such as couplers and phase shifters. Fig. 14(b) displays the complete beamforming system with the top layer included.

The reflection coefficients and isolations between the input ports of the beamforming system are plotted in Figs. 14(c–f). The results demonstrate that the beamforming network covers entire upper area of the Ka-band ranging from 30 to 40 GHz when its input ports are excited.

In addition to excellent broadband reflection coefficients (better than −15 dB), the design achieves high isolation between the input ports (exceeding 15 dB), ensuring effective decoupling and stable multi-port operation. This performance enables high radiation gain at 38 GHz, as shown in Fig. 14(g). The radiation patterns are highly directive, demonstrating wide-angle beam scanning capability.

A slight performance degradation is observed when the Nolen matrix is integrated with the input feeding transition and slot-array antennas. While the components were individually optimized, cascading them introduces inevitable mechanical and electromagnetic discontinuities, including tolerances in the GGW pins and air gap, surface roughness, and minor misalignments at the interfaces. Additionally, once the slot-array antenna is connected, the output ports no longer terminate into ideal matched loads but instead into a radiating structure that exhibits mutual coupling, producing small amplitude and phase perturbations, particularly along longer routing paths. Nevertheless, the resulting degradation remains minimal, with return loss and inter-port isolation better than 15 dB, amplitude variation within ±1.2 dB, and phase error within ±10° near 38 GHz, demonstrating that the integrated system successfully retains the intended broadband beamforming performance.

G. MEASUREMENT SET-UP AND EXPERIMENTAL VALIDATION

The fabricated Nolen matrix-based beamforming network is exhibited in Fig. 15. The measurements are conducted in an anechoic chamber to minimize reflections and external electromagnetic interference. The chamber, shown in Fig. 15, is lined with absorbing material (blue pyramidal foam) to simulate free-space conditions, ensuring the accuracy of the S-parameter and radiation pattern measurements. The proposed beamforming system was mounted securely on a

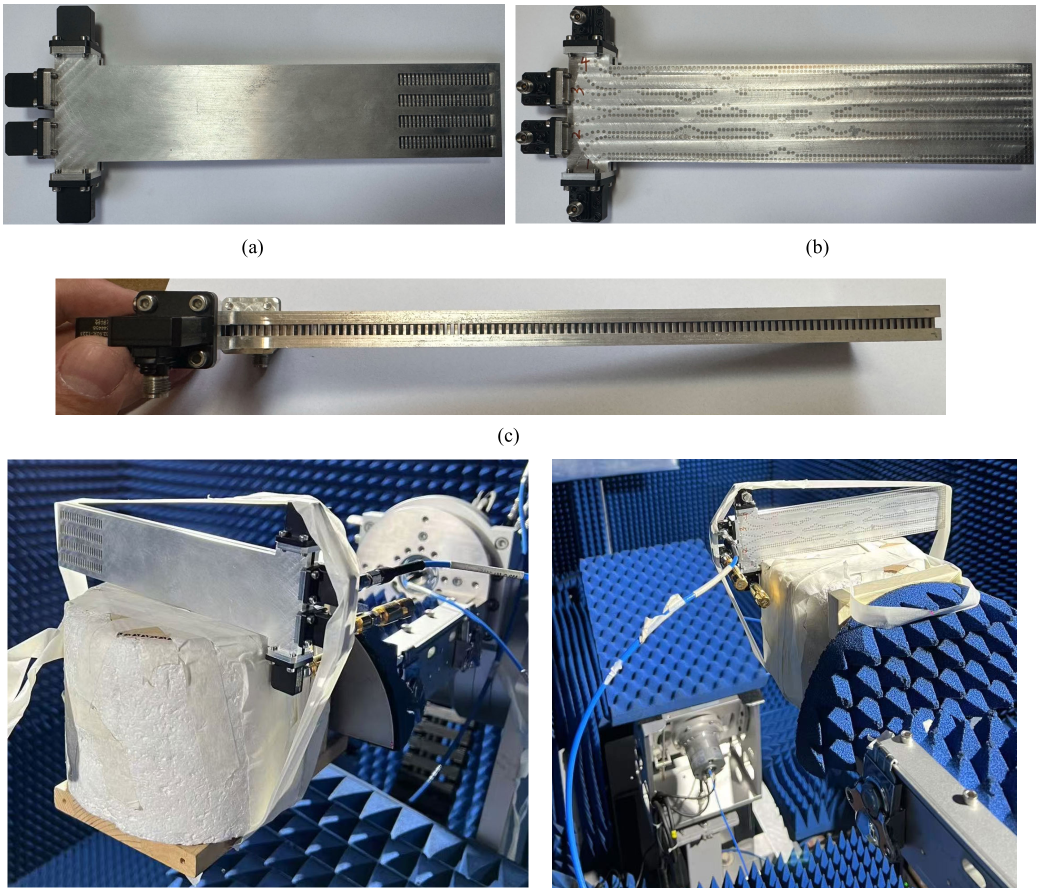

FIGURE 15. The fabricated Nolen matrix-based beamforming network, (a) top-, (b) bottom-, and (c) side-view. (d) The measurement set-up.

positioning stage for precise alignment with the measurement equipment. WR28 waveguide flange adapter was used to feed the input ports of the beamforming network. The ports are excited sequentially or simultaneously, depending on the S-parameter measurement requirements. A high-frequency VNA was used to measure the S-parameters of the system across the target frequency range of 30–40 GHz. Calibration of the VNA and other equipment is performed prior to the measurements to ensure accurate S-parameter readings. The VNA was connected to the input and output ports of the DUT via precision coaxial cables and waveguide adapters to ensure minimal loss and high measurement accuracy. A calibrated receiving antenna is located at a specific distance from the DUT to measure radiation patterns and verify beamforming performance. The position of the receiving antenna can be adjusted to capture the radiation characteristics in various directions.

The plots in Figs. 16 (a)–(d) illustrate the experimental and simulated S-parameters for Ports 1 – 4. The reflection coefficients show that good impedance matching is achieved primarily around the design frequency of 38 GHz. However, Ports 2 and 3 exhibit noticeable degradation, with several frequency regions where $|S_{11}|$ exceeds −10 dB in both simulation and measurement, indicating reduced impedance matching in those bands. The transmission coefficients represent the well-defined separation with predictable behavior between the Ports. Simulated results exhibit expected coupling levels showing consistent performance and proper power distribution demonstrating effective signal control and phase alignment. The measured data closely follow the simulated trends in terms of overall shape and null locations but display minor deviations, such as ripples and slight frequency shifts. These discrepancies are likely due to fabrication imperfections, measurement setup tolerances, practical measurement limitations, and assembly imperfections. Overall, the ports demonstrate acceptable reflection and transmission characteristics, with optimal performance near the design frequency of 38 GHz.

It should be noted that the S-parameters in Fig. 16(a–d) are plotted with an extended vertical scale down to −40 dB for completeness. However, when evaluated using the conventional $|S_{11}| < -10$ dB criterion, the effective impedance bandwidth is reduced and varies across ports.

The measured radiation pattern of the proposed beamforming network is shown on Fig. 16(e), while the simulated radiation pattern is presented on Fig. 14. Both sets of patterns

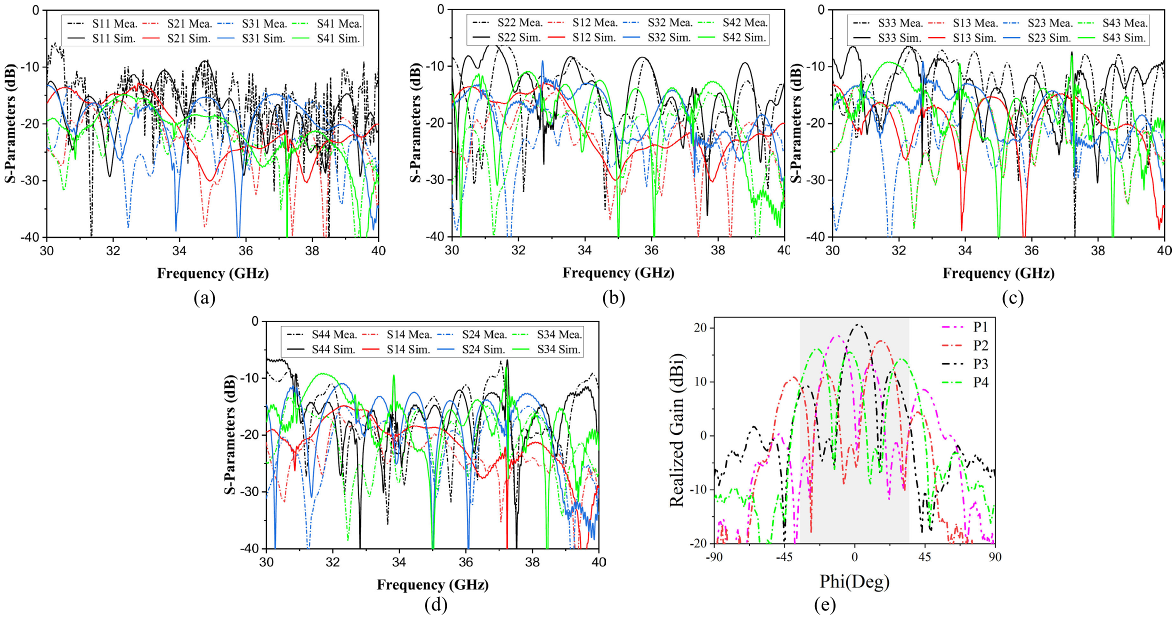

FIGURE 16. The simulated and experimantal S-parameters of the proposed Nolen matrix-based beamforming network, (a) Port 1, (b) Port 2, (c) Port 3, and (d) Port 4. (e) Experimantal radiation patterns at 38 GHz.

exhibit multiple lobes with a generally similar structure, indicating good consistency between the simulation and experimental results. However, some differences are evident. The main lobes in both the simulated and measured patterns are aligned near the central angle (Phi = 0°), demonstrating the network's beamforming capability. Secondary lobes in the measured patterns show slight deviations in position and magnitude compared to the simulated patterns. Additionally, the gain values in the simulated patterns are higher overall, with sharper peaks in both the main and secondary lobes. In contrast, the measured patterns exhibit smoother variations and slightly reduced peak gains, likely due to practical factors such as fabrication imperfections, material losses, or inefficiencies in the measurement setup. Another notable observation is the symmetrical patterns. While the simulated results are more symmetrical around Phi = 0°, the measured results display minor asymmetry, especially in the side lobes. This asymmetry could be attributed to real-world variations in the experimental setup or minor misalignments during testing.

While Port 1 demonstrates the most favorable return loss and consistent radiation performance, the characteristics of Ports 2, 3, and 4 show moderate degradation. This discrepancy is mainly attributed to practical implementation challenges such as physical asymmetries in the GGW layout, sensitivity to fabrication tolerances, and minor mismatches between the matrix outputs and the slotted array antenna inputs. These effects become more prominent along the off-center paths of the matrix. In future work, improvements in layout symmetry and tighter control of manufacturing tolerances will be pursued to enhance uniformity across all output ports.

III. COMPARISON WITH PRIOR ARTS

In this section, the proposed beamforming system is evaluated against representative Nolen matrix implementations reported in the literature, with particular emphasis on recent mmWave and high-frequency designs to enable a meaningful like-for-like comparison. The evaluation considers key parameters including topology, design method, matrix size, bandwidth, design frequency, reflection coefficient, isolation between input ports, and design complexity and planarity, as summarized in Table 6. Furthermore, the proposed design operates at 38 GHz, which is significantly higher than many reported Nolen matrix implementations, thereby demonstrating feasibility at mmWave frequencies where losses and phase errors are more critical. The proposed design spans a wide design bandwidth of 30–40 GHz; however, the effective impedance bandwidth, defined by $|S_{11}| < -10$ dB, is narrower and varies across ports, with optimal performance concentrated around 38 GHz.

The design spans 30–40 GHz (28.5%) in terms of physical structure; however, optimal performance is concentrated around 38 GHz. The usable beamforming bandwidth is therefore concentrated around the design frequency of 38 GHz, where amplitude balance, phase progression, and matching conditions are simultaneously satisfied. This performance is competitive among reported mmWave Nolen matrix implementations. Although [34], [35], [41], and [42] provide wideband design capability, but they operate at lower frequencies (1.8 and 3 GHz), which are not suitable for mm-wave applications. The proposed design demonstrates competitive performance within the mmWave regime, particularly at 38 GHz, where amplitude balance, phase accuracy, and impedance matching are simultaneously achieved. This

TABLE 6. Comparison of reported Nolen matrix implementations. Bandwidth values are reported according to the definitions provided in the original references (typically $|S_{11}| < -10$ dB where specified). Comparisons across different technologies and frequency ranges reflect trade-offs in performance, loss, and integration rather than direct equivalence.

Ref.	Technology	Center Freq. (GHz)	Matrix Size	Bandwidth (%)	Phase Error (°)	Isolation (dB)	Validation	Structure
[29]	SIW	12.5	4×4	8	±12.5	Not reported	Sim. + Meas.	Planar (SIW)
[33]	Microstrip	5.8	3×3	8	±5.8	Not reported	Sim.	Planar (microstrip)
[34]	Microstrip	1.8	4×4	41.5	±1.1	Not reported	Sim.	Planar (microstrip)
[38]	Microstrip	5.8	3×3	5.03	±1.6	Not reported	Sim.	Planar (microstrip)
[40]	SIW	77	4×4	11.7	±1.0	Not reported	Sim. + Meas.	Planar (SIW)
[43]	Microstrip	3.0	4×4	10.17	±2.5	Not reported	Sim.	Planar (microstrip)
[44]	Microstrip	2.2	4×4	9.3	±0.9	Not reported	Sim.	Planar (microstrip)
This Work	GGW	38	4×4	30–40 GHz (design range); effective bandwidth narrower ($|S_{11}| < -10$ dB)	±10	>15	Sim. + Meas.	Single-layer GGW

*Bandwidth values are reported based on available definitions in the literature (typically $|S_{11}| < -10$ dB where specified). Differences in reported criteria may limit direct comparison.

frequency is notably higher than most designs compared, which generally operate below X-band (12 GHz), except for [37], [39], [40], [45], [46], and [48].

The proposed design features a planar and single-layer configuration, simplifying the fabrication process and reducing production costs. It should be noted that, unlike microstrip-based implementations, the GGW structure does not primarily aim to minimize footprint; instead, it provides advantages in terms of reduced loss, improved isolation, and robustness at mmWave frequencies. While GGW structures require high fabrication precision, particularly in maintaining uniform pin geometry and air gaps, they eliminate the need for multilayer alignment and provide improved electromagnetic performance at mmWave frequencies, representing a trade-off between manufacturing tolerance and performance. This design approach contrasts with multilayer or more complex topologies used in other systems [33], [36], [37], [42], [43], [44], [45], [46], [47], [48], [49]. The planar design contributes to ease of integration and lower complexity, making the system more accessible and cost-effective.

The straightforward topology of the proposed design minimizes complexity and cost, providing an economical solution compared to more intricate designs. For example, systems in [34] and [41] use complex methods like SFGs, and bandpass filters, respectively. The simplicity of the proposed design facilitates easier manufacturing and integration contributing to its durability and consistent operation. The proposed system's robustness ensures reliable performance under various conditions.

The proposed beamforming system provides high bandwidth, competitive phase accuracy (±10°), and simple planar design making it particularly well-suited for terrestrial and space telecommunications, and 5G communication systems.

It is also important to highlight that, unlike the GGW-based Nolen matrix reported in [21], which is based on a multilayer structure and limited to simulation, the proposed design is realized in a single-layer configuration and experimentally validated as a complete beamforming system.

Quantitatively, the proposed design achieves return loss better than −15 dB, port isolation exceeding 15 dB, amplitude imbalance within ±1.2 dB, and phase error within ±10°, demonstrating competitive performance among state-of-the-art mmWave beamforming networks.

IV. CONCLUSION

This paper investigated the design, fabrication, and experimental validation of an integrated single-layer 4 × 4 Nolen matrix beamforming network implemented in groove gap waveguide (GGW) technology and optimized for operation around 38 GHz within the upper Ka-band. Broadband H-plane directional couplers and phase shifters were combined in a predominantly parallel routing topology, and dedicated delay-compensation sections were introduced to correct residual path-length disparities while preserving a compact footprint. An input-feeding transition compatible with WR-28 waveguide interfaces was incorporated without disturbing the intended amplitude and phase relationships. A linear GGW slot-array antenna was integrated to validate multi-beam radiation and wide-angle scanning. While the structure spans the 30–40 GHz range, the effective impedance bandwidth is narrower and varies across ports, with best performance observed near 38 GHz.

In contrast to prior Nolen matrix implementations, including the GGW-based multilayer design in [21], which is limited to simulation results, the proposed work provides a fully single-layer realization with complete experimental validation and system-level integration. The design incorporates built-in delay compensation, achieves improved phase accuracy ($\pm 10^\circ$), and supports practical integration with a radiating array. Measurements confirm return loss better than -15 dB, port-to-port isolation exceeding 15 dB, amplitude imbalance within ± 1.2 dB, and phase error within $\pm 10^\circ$, with stable phase progression around the design frequency and only modest degradation at the band edges due to practical assembly tolerances. These results demonstrate that the proposed approach offers a viable path toward broadband mmWave multi-beam front ends for satellite-oriented communication systems.

Compared to existing mmWave Nolen matrix implementations, the proposed approach provides a practical balance between performance, structural simplicity, and system-level integration, addressing key limitations of prior designs.

As observed in Table 6, many reported Nolen matrix implementations operate at lower frequencies or rely solely on simulation results. In contrast, the proposed design demonstrates a fully measured implementation at 38 GHz, highlighting its feasibility for mmWave applications where loss, fabrication tolerance, and phase stability become more critical.

These characteristics make the proposed beamforming network particularly suitable for satellite-oriented multi-beam systems operating in the upper Ka-band.

Future work will explore the integration of GGW-based beamforming networks with reconfigurable radiating structures such as leaky-wave and pinching antennas to further enhance beam agility and spatial multiplexing capabilities.

REFERENCES

[1] S. Zargari, D. Galappaththige, and C. Tellambura, "Transmit power-efficient beamforming design for integrated sensing and backscatter communication," *IEEE Open J. Commun. Soc.*, vol. 6, pp. 775–792, 2025, doi: 10.1109/OJCOMS.2025.3527860.

[2] A. Salih and S. Al-Dharrab, "Spectral efficiency and hybrid beamforming for multi-user in airborne integrated sensing and communication systems," *IEEE Open J. Commun. Soc.*, vol. 6, pp. 1190–1201, 2025, doi: 10.1109/OJCOMS.2025.3533358.

[3] P. Kanani, M. J. Omidi, M. Modarres-Hashemi, and H. Yanikomeroglu, "HAPS-ISAC: Enhancing sensing and communication in 6G networks with advanced MIMO beamforming," *IEEE Open J. Commun. Soc.*, vol. 6, pp. 5988–6004, 2025, doi: 10.1109/OJCOMS.2025.3587077.

[4] A. Saifaldawla, F. Ortiz, E. Lagunas, and S. Chatzinotas, "Attention-based blind adaptive receive beamforming for interference limited NGSO satellite systems," *IEEE Open J. Commun. Soc.*, vol. 6, pp. 8946–8964, 2025, doi: 10.1109/OJCOMS.2025.3622661.

[5] D. Salakhov, N. Zlatanov, A. Frolov, and M. K. Hanawal, "TTD-based hybrid beamforming for multi-user near-field communications: A Riemannian optimization approach," *IEEE Open J. Commun. Soc.*, vol. 7, pp. 583–597, 2026, doi: 10.1109/OJCOMS.2026.3651840.

[6] I. Batool, M. M. Fouda, M. Ismail, M. I. Ibrahem, Z. Md Fadlullah, and N. Kato, "Quantum-enhanced massive MIMO beamforming for 6G IoT networks: A QAOA-based optimization framework," *IEEE Open J. Commun. Soc.*, vol. 7, pp. 222–238, 2026, doi: 10.1109/OJCOMS.2025.3645207.

[7] A. K. Vallappil, M. K. A. Rahim, B. A. Khawaja, N. A. Murad, and M. G. Mustapha, "Butler matrix based beamforming networks for phased array antenna systems: A comprehensive review and future directions for 5G applications," *IEEE Access*, vol. 9, pp. 3970–3987, 2021.

[8] P. Angeletti and M. Lisi, "Multimode beamforming networks for space applications," *IEEE Antennas Propag. Mag.*, vol. 56, no. 1, pp. 62–78, Feb. 2014.

[9] G. Rosati and J. Munn, "Fast prototyping of an 8×8 Butler matrix beamforming network for 5G applications," in *Proc. Int. Conf. Electromagn. Adv. Appl. (ICEAA)*, 2017, pp. 1029–1032.

[10] P. S. Hall and S. J. Vetterlein, "Review of radio frequency beamforming techniques for scanned and multiple beam antennas," *IEE Proc. H-Microw., Antennas Propag.*, vol. 137, no. 5, pp. 293–303, Oct. 1990.

[11] S. Vashist, M. K. Soni, and P. K. Singhal, "A review on the development of Rotman lens antenna," *Chin. J. Eng.*, vol. 14, no. 11, pp. 1–9, 2014. [Online]. Available: https://www.hindawi.com/journals/cje/2014/385385/

[12] M. Ansari, B. Jones, H. Zhu, N. Shariati, and Y. J. Guo, "A highly efficient spherical Luneburg lens for low microwave frequencies realized with a metal-based artificial medium," *IEEE Trans. Antennas Propag.*, vol. 69, no. 7, pp. 3758–3770, Jul. 2021.

[13] J. Ruze, "Wide-angle metal-plate optics," *Proc. IRE*, vol. 38, no. 1, pp. 53–59, Jan. 1950.

[14] W. Rotman and R. Turner, "Wide-angle microwave lens for line source applications," *IEEE Trans. Antennas Propag.*, vol. AP-11, no. 6, pp. 623–632, Nov. 1963.

[15] J.-W. Lian, Y.-L. Ban, H. Zhu, and Y. J. Guo, "Reduced-sidelobe multibeam array antenna based on SIW Rotman lens," *IEEE Antennas Wireless Propag. Lett.*, vol. 19, pp. 188–192, 2020.

[16] J. Blass, "Multidirectional antenna–A new approach to stacked beams," in *Proc. IRE Int. Conv. Rec.*, vol. 8, New York, NY, USA, 1960, pp. 48–50, doi: 10.1109/IRECON.1960.1150892.

[17] J. Nolen, "Synthesis of multiple beam networks for arbitrary illuminations," Ph.D. dissertation, Bendix Corp., Baltimore, MD, USA, Apr. 1965.

[18] N. J. G. Fonseca, "Printed S-band 4×4 Nolen matrix for multiple beam antenna applications," *IEEE Trans. Antennas Propag.*, vol. 57, no. 6, pp. 1673–1678, Jun. 2009.

[19] J. K. Butler, "Beam-forming matrix simplifies design of electronically scanned antennas," *Electron. Des.*, vol. 9, no. 8, pp. 170–173, 1961.

[20] H. Moody, "The systematic design of the Butler matrix," *IEEE Trans. Antennas Propag.*, vol. 12, no. 6, pp. 786–788, Nov. 1964.

[21] N. Castro et al., "Gap waveguide cruciform couplers nolen matrix for multi beam antenna at 38 GHz," in *Proc. IEEE AP-S/URSI*, Jul. 2023, pp. 23–28.

[22] M. Alibakhshikenari, B. Virdee, H. Zakeri, E. Limiti, and T. Saber, "Design guidelines using groove gap-waveguide technology for realizing a millimeter-wave 4×4 Butler beamforming matrix for space multiplexing," in *Proc. Asia–Pacific Microw. Conf. (APMC)*, Dec. 2025, pp. 1–3, doi: 10.1109/APMC65046.2025.11378003. [Online]. Available: https://www.apmc2025.org/invited

[23] P.-S. Kildal, E. Alfonso, A. Valero-Nogueira, and E. Rajo-Iglesias, "Local metamaterial-based waveguides in gaps between parallel metal plates," *IEEE Antennas Wireless Propag. Lett.*, vol. 8, pp. 84–87, 2009.

[24] W. Y. Yong, A. Vosoogh, A. Bagheri, C. Van De Ven, A. Hadaddi, and A. A. Glazunov, "An overview of recent development of the gap-waveguide technology for mmWave and sub-THz applications," *IEEE Access*, vol. 11, pp. 69378–69400, 2023.

[25] E. Rajo-Iglesias, M. Ferrando-Rocher, and A. U. Zaman, "Gap waveguide technology for millimeter-wave antenna systems," *IEEE Commun. Mag.*, vol. 56, no. 7, pp. 14–20, Jul. 2018.

[26] Y. Shi et al., "Gap waveguide technology: An overview of millimeter-wave circuits based on gap waveguide technology using different fabrication technologies," *IEEE Microw. Mag.*, vol. 24, no. 1, pp. 62–73, Jan. 2023.

[27] M. Alibakhshikenari et al., "6G mm-wave Nolen-matrix beamformer using groove gap-waveguide technology for tracking space targets and satellite global connectivity through IoT," *Results Eng.*, vol. 30, Jun. 2026, Art. no. 110572.

[28] M. Alibakhshikenari et al., "Matrix-based millimeter-wave beamforming networks using groove gap-waveguide technology for satellite space multiplexing," in *Proc. IEEE Conf. Antenna Meas. Appl. (CAMA)*, France, Nov. 2025, pp. 1–4.

[29] T. Djerafi, N. J. G. Fonseca, and K. Wu, "Planar Ku-band 4×4 Nolen matrix in SIW technology," *IEEE Trans. Microw. Theory Techn.*, vol. 58, no. 2, pp. 259–266, Feb. 2010.

[30] E. Rajo-Iglesias and P.-S. Kildal, "Numerical studies of bandwidth of parallel-plate cut-off realised by a bed of nails, corrugations and mushroom-type electromagnetic bandgap for use in gap waveguides," *IET Microw., Antennas Propag.*, vol. 5, no. 3, pp. 282–289, Feb. 2011.

[31] S. I. Shams and A. A. Kishk, "Double cone ultra wide band unit cell in ridge gap waveguides," in *Proc. IEEE Antennas Propag. Soc. Int. Symp. (APSURSI)*, Jul. 2014, pp. 1768–1769.

[32] E. Rajo-Iglesias, P.-S. Kildal, A. U. Zaman, and A. Kishk, "Bed of springs for packaging of microstrip circuits in the microwave frequency range," *IEEE Trans. Compon., Packag., Manuf. Technol.*, vol. 2, no. 10, pp. 1623–1628, Oct. 2012.

[33] Y. Yang et al., "Analytical design method and implementation of broadband 4 × 4 Nolen matrix," *IEEE Trans. Microw. Theory Techn.*, vol. 70, no. 1, pp. 343–355, Jan. 2022.

[34] H. Zhu, M. Ansari, and Y. J. Guo, "Wideband beam-forming networks utilizing planar hybrid couplers and phase shifters," *IEEE Trans. Antennas Propag.*, vol. 70, no. 9, pp. 7592–7602, Sep. 2022.

[35] A. Imani and M. S. Bayati, "A novel design of compact broadband 4 × 4 Butler matrix-based beamforming antenna array for C-band applications," *AEU-Int. J. Electron. Commun.*, vol. 138, 2021.

[36] C. Lee, M. K. Khattak, and S. Kahng, "Wideband 5G beamforming printed array clutched by LTE-A 4×4-multiple-input–multiple-output antennas with high isolation," *IET Microw., Antennas Propag.*, vol. 12, no. 8, pp. 1407–1413, Jul. 2018.

[37] P. Li, H. Ren, and B. Arigong, "A symmetric beam-phased array fed by a Nolen matrix using 180° couplers," *IEEE Microw. Wireless Compon. Lett.*, vol. 30, no. 4, pp. 387–390, Apr. 2020.

[38] S. Trinh-Van et al., "A sidelobe-reduced, four-beam array antenna fed by a modified 4×4 Butler matrix for 5G applications," *IEEE Trans. Antennas Propag.*, vol. 67, no. 7, pp. 4528–4536, Jul. 2019.

[39] T. Djerafi, N. J. G. Fonseca, and K. Wu, "Broadband substrate integrated waveguide 4×4 Nolen matrix based on coupler delay compensation," *IEEE Trans. Microwave Theory Techn.*, vol. 59, no. 7, pp. 1740–1745, Jul. 2011.

[40] K.-R. Xiang et al., "A broadband 3×4 Butler matrix and its application in multibeam antenna arrays," *IEEE Trans. Antennas Propag.*, vol. 67, no. 12, pp. 7622–7627, Dec. 2019.

[41] Q. P. Chen, Z. Qamar, S. Y. Zheng, Y. Long, and D. Ho, "Design of a compact wideband Butler matrix using vertically installed planar structure," *IEEE Trans. Compon., Packag., Manuf. Technol.*, vol. 8, no. 8, pp. 1420–1430, Aug. 2018.

[42] F. E. Fakoukakis and G. A. Kyriacou, "Novel Nolen matrix based beamforming networks for series-fed low SLL multibeam antennas," *Prog. Electromagn. Res. B*, vol. 51, pp. 33–64, 2013.

[43] N. J. G. Fonseca, "Printed S-band 4 × 4 Nolen matrix for multiple beam antenna applications," *IEEE Trans. Antennas Propag.*, vol. 57, no. 6, pp. 1673–1678, Jun. 2009.

[44] H. Ren et al., "A novel 2-D 3×3 Nolen matrix for 2-D beamforming applications," *IEEE Trans. Microwave Theory Techn.*, vol. 67, no. 11, pp. 4622–4631, Nov. 2019.

[45] W. Sun et al., "A miniaturized wideband 4×8 Butler matrix for beamforming in millimeter-wave applications," *IEEE Trans. Microwave Theory Techn.*, vol. 71, no. 10, pp. 4588–4599, Oct. 2023.

[46] Y. Lee, B. Suh, and B.-W. Min, "A Ka-band bi-directional reconfigurable switched beam-forming network based on 4 × 4 Butler matrix in 28-nm CMOS," *IEEE Trans. Microw. Theory Techn.*, vol. 71, no. 6, pp. 2479–2487, Jun. 2023.

[47] Q. Shao et al., "Design of 4×4 and 8 × 8 filtering Butler matrices utilizing combined 90° and 180° couplers," *IEEE Trans. Microw. Theory Techn.*, vol. 69, no. 8, pp. 3842–3852, Aug. 2021.

[48] Z. Yin, H. Zhu, X. Lv, J. Lai, and Y. Yang, "3-D-printed ultracompact Butler matrix for wideband millimeter-wave beamforming," *IEEE Trans. Microw. Theory Techn.*, vol. 73, no. 9, pp. 5953–5965, Sep. 2025.

[49] K. Han, G. Wei, M. Wang, T. Qiu, and S. Lei, "Design of modified Butler matrix based on N-way directional coupler and its multibeam application," *IEEE Trans. Microw. Theory Techn.*, vol. 71, no. 4, pp. 1654–1662, Apr. 2023.

MOHAMMAD ALIBAKHSHIKENARI (Member, IEEE) was born in Mazandaran, Iran, in February 1988. He received the Ph.D. degree (European Label and cum laude) in electronics engineering from the University of Rome "Tor Vergata" (UNITOV), Italy, in February 2020. From May 2018 to December 2018, he was a Ph.D. Visiting Researcher with the Chalmers University of Technology, Gothenburg, Sweden. His training during this visit included a research stage at Swedish Company "Gap Waves AB." During the Ph.D. degree (November 2016–February 2020), he was recognized as the Winner of 13 grants for attending the doctoral schools organized by European School of Antennas (ESoA, 5), European Doctoral Programs in Metamaterials (EUPROMETA, 3), European Microwave Conference (EuMC, 2), Società Italiana di Elettronica—Italian Society of Electronics (SIE, 1), ITMO University (Nanophotonics and Metamaterials, 1), Aix-Marseille Université (Metamaterials, 1), which were held in various European universities. He successfully achieved all 30 credits provided by doctoral schools leading him to obtain his Ph.D. degree with European Label. He is currently a Marie Sklodowska-Curie, ROSETTA, and Lero (the Research Ireland Centre for Software) Post-Doctoral Fellow with the University of Galway, Ireland. As part of this fellowship, he has five research visits at the Microwave Engineering Center for Space Applications (MECSA), in October 2025; the Universitat Ramon Llull, Barcelona, Spain, in October 2025; the Institute of Science Tokyo, Japan, in November 2025; Pusan National University, Busan, South Korea, in December 2025; and Sogang University, Seoul, South Korea, in December 2025. From September 2024 to June 2025, he was with UNITOV as a Senior Researcher. From July 2021 to August 2024, he was with the Department of Signal Theory and Communications, Universidad Carlos III de Madrid (uc3m), Spain, as a Marie Sklodowska-Curie and a CONEX-Plus Fellow. During this program, he has spent two secondments at the Microwave Engineering Center for Space Applications (MECSA), Rome, Italy, from April to August 2024; and SARAS Technology Ltd., Company, Leeds, U.K., from December 2022 to May 2023. In addition, during this program, he has one-week research visits at the University of Catania, Italy, in May 2024, along with an invited lecture titled "Terahertz Antennas-Based on Metasurface and SIW" for the master's and Ph.D. students, and post-doctoral researchers; University of Messina, Italy, in May 2024; University of Bradford, U.K., in May 2023; and Edinburgh Napier University, U.K., in April 2023. In May 2026, he received a letter of acknowledgement from President of the University of Galway, "Prof. David Burn," and he was commended due to his contribution to the research excellence of the university. In 2021 and 2022, he received the letter of acknowledgement from the Vice-Rector of studies of the Universidad Carlos III de Madrid, "Prof. Marta Pilar Macias Dorissa," due to his contribution to the teaching excellence in the "electromagnetic fields." In November 2019, he was a Winner of a Post-Doctoral Research Fund for two years awarded by UNITOV. His research interests include electromagnetic fields, antennas and wave-propagations, metamaterials and metasurfaces, RF/microwave systems, sensors, next generation of wireless communications, multiple input multiple output (MIMO) systems, millimeter-waves and terahertz devices, and beamforming networks. His research activities are documented in about 200 articles published in international journals, two books, ten book chapters, and about 112 papers in proceedings of international conferences, including 49 in-person presentations in 31 conferences and 27 on-line presentations in 13 conferences (the rest were presented by his colleagues). His research works received more than 9 700 citations with an H-index above 59 reported by Scopus, Google Scholar, and ResearchGate. According to Stanford University yearly analysis, he has been among the World's Top 2% Scientists of highly cited scientific authors, since 2020. He was listed in both Career Long and Single Year Impact in Stanford's list. He is a member of the Reviewer Panel of Dutch Research Council (NWO), U.K. Research and Innovation (UKRI) Funding Service, and IEEE MTT-S Education Committee Fellowships and Scholarships; and the External Examiner of several Ph.D. dissertations from various worldwide universities. He was a recipient of two Young Engineer Awards of 47th and 48th European Microwave Conferences held in Nuremberg, Germany in 2017 and in Madrid, Spain, in 2018, respectively. In April 2020, his research article titled "High-Gain Metasurface in Polyimide On-Chip Antenna Based on CRLH-TL for Sub Terahertz Integrated Circuits," (Scientific Reports, volume 10, Article number 4298, in 2020) was awarded as the Best Month Paper at the University of Bradford. In addition, he serves as an Associate Editor for two scientific journals of *Radio Science* and *The Journal of Engineering* (IET). He acts as a referee in several journals. He is also the technical program committee (TPC) member and the session chair of several international conferences.

BAL VIRDEE (Senior Member, IEEE) received the B.Sc. and M.Phil. degrees in communications engineering from the University of Leeds, U.K., in 1986 and 1989, respectively, and the Ph.D. degree in electronic engineering from the University of London, London, U.K., in 1996. He has worked in industry for various companies, including Philips (U.K.) as a Research and Development-Engineer and Teledyne Defence and Space as a Future Products Developer in RF/microwave communications. He has taught at several academic institutions before joining London Metropolitan University, where he is currently a Senior Professor of communications technology with the School of Computing and Digital Media. He is also the Head of the Communications Technology Research Center. His research, in collaboration with industry and academia, is in wireless communications encompassing mobile-phones to satellite-technology. He is an Executive Member of IET's Technical and Professional Network Committee on RF/microwave technology. He is a fellow of IET. He has chaired technical sessions at IEEE international conferences and published several research papers.

YAZEED MOHAMMAD QASAYMEH received the B.Sc. (Eng.) degree from Mutah University, Kerak, Jordan, in 2006, the M.Sc. (Eng.) degree in engineering from the College of Electrical and Computer Engineering, Universiti Sains Malaysia, Penang, Malaysia, in 2009, and the Ph.D. degree from the College of Electrical and Electronic Engineering, Universiti Sains Malaysia. He is currently an Associate Professor with the College of Engineering, Majmaah University, Saudi Arabia. His research interests include antennas array, wireless communication MIMO, and distributed antenna systems.

ALI ZIDOUR was born in Chlef, Algeria, in 1988. He received the M.S. degree in telecommunication engineering from the Hassiba Benbouali University of Chlef in 2015, and the Ph.D. degree in electrical systems engineering from M'hammed Bougara University, Boumerdes, in 2025. His current research interests include electromagnetic systems, microwave circuits, millimeter-wave antenna arrays, programmable metasurfaces, and reconfigurable intelligent surfaces.

MUHAMMAD AKMAL CHAUDHARY received the master's and Ph.D. degrees in electrical and electronic engineering from Cardiff University, Cardiff, U.K., in 2007 and 2011, respectively, and the M.B.A. degree in leadership and corporate governance from Edinburgh Business School, Heriot-Watt University, Edinburgh, U.K., in 2022. Prior to joining Ajman University, United Arab Emirates, in 2012, he held a post-doctoral research position with the Centre for High Frequency Engineering, Cardiff University, where he has conducted commercial work for Freescale Semiconductor, Mesuro, TriQuint Semiconductor, National Physical Laboratory (NPL), and GaN Systems. His research interests include nonlinear device characterization, spectrum-efficient power amplifiers, modulated measurement techniques, and microwave electronics have led to over 150 academic publications. He is a Chartered Engineer with the Engineering Council, U.K.; and a fellow of the Higher Education Academy, U.K.

CHAN HWANG SEE (Senior Member, IEEE) received the B.Eng. degree (Hons.) in electronic, telecommunication and computer engineering and the Ph.D. degree from the University of Bradford, U.K., in 2002 and 2007, respectively. He is currently a Professor of antennas and applied electromagnetics with the School of Computing, Engineering and the Built Environment, Edinburgh Napier University, U.K. He was the Head of electrical engineering and mathematics with Edinburgh Napier University, from 2019 to 2022. His research interests include wireless sensor network system design, computational bioelectromagnetics, antennas, microwave circuits, the Internet of Things (IoTs), microwave sensors, wireless power transfer (WPT), and microwave energy harvesting. He has published over 250 peer-reviewed journal articles and conference papers in these research areas. He is the co-author for one book and three book chapters. Since 2023, he has been serving as the U.K. Representative for Commission K: Electromagnetics in Biology and Medicine within the International Union of Radio Science (URSI). He is a Full Member of the EPSRC Review College. He is a Chartered Engineer and a fellow of the Institution of Engineering and Technology. He is also a fellow of the Higher Education Academy. He received the IEEE Malaysia AP/MTT/EMC Joint Chapter Best Paper Award in 2020. He was a recipient of the two Young Scientist Awards from the International Union of Radio Science (URSI) and Asia-Pacific Radio Science Conference (AP-RASC) in 2008 and 2010, respectively. In 2009, he received the Certificate of Excellence for his successful Knowledge Transfer Partnership (KTP) with Yorkshire Water, for the design and implementation of a wireless sensor system for sewerage infrastructure monitoring. He is an Associate Editor of IEEE ACCESS and an Editor of *Journal of Electronics and Electrical Engineering*, *Scientific Reports*, *PeerJ Computer Science*, and *Frontiers in Antennas and Propagation Metamaterial Antennas and Wireless Power Transfer*. According to Web of Science, he has completed over 500 verified reviews and over 250 verified editor records.

PATRIZIA LIVRERI (Senior Member, IEEE) received the Laurea degree (Hons.) in electronics engineering and the Ph.D. degree in electronics and communications engineering from the University of Palermo, Italy, in 1986 and 1992, respectively. From 1993 to 1994, she was a Researcher with the National Council for Researches (CNR), Rome, Italy. Since 1995, she has been the Scientific Director for the Microwave Instruments and Measurements Laboratory, Department of Engineering, University of Palermo. In 2020, she also joined the CNIT National Laboratory for Radar and Surveillance Systems (RaSS), Pisa. She is currently a Professor with the Department of Engineering, University of Palermo, and a Visiting Professor with San Diego State University. She is also a Principal Investigator of the "Microwave Quantum Radar" Project, funded by the Ministry of Defense, in 2021. She is the author or co-author of more than 250 publications in prestigious international journals and conferences. Her research interests include microwave and millimeter vacuum high power (TWT, Klystron) and solid-state power amplifiers for radar applications, high power microwave sources (virtual cathode oscillator and magnetically insulated transmission line oscillator), microwave and optical antennas, radar, and microwave quantum radar. In 2024, she has been nominated as an IEEE Aerospace and Electronic Systems Distinguished Lecturer.

NISAR AHMAD ABBASI received the B.Sc. degree (Hons.) in electrical and electronic engineering from the University of Engineering and Technology, Peshawar, Pakistan, in 2001, and the M.Sc. and Ph.D. degrees in electronic engineering from The University of Sheffield, Sheffield, U.K., in 2007 and 2011, respectively. He has held various positions, such as an Assistant Manager, the Manager, and the General Manager, while working for the Ministry of Science, Pakistan, from 2001 to 2016. He was an Assistant Professor with the University of Hafr Al Batin, Hafr Al Batin, Saudi Arabia, from 2017 to 2025. He is currently an Associate Professor with Bahrain Polytechnic, Bahrain. His research interests include the design and analysis of various antenna types and telecommunication networks. He is a Professional Engineer (P.E.) in Pakistan and a member of the Pakistan Engineering Council (PEC).

MOHAMADARIFF OTHMAN (Member, IEEE) received the B.Eng. degree (Hons.) in electronic engineering from Multimedia University, Malaysia, in 2006, and the M.Sc. degree in RF and microwave and the Ph.D. degree in antenna and propagation from the Universiti Sains Malaysia (USM), Malaysia, in 2008 and 2015, respectively. He has been with the Department of Electrical Engineering, Universiti Malaya, Malaysia, as a Senior Lecturer, since 2016. Prior to that, he was a Lecturer with UCSI University, Malaysia, for almost 1.5 years. His research interests include 5G antennas, dielectric characterization, dielectric resonator antenna design, and antenna design optimization. He is a member of the Board of Engineers Malaysia.

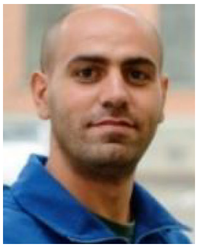

TAKFARINAS SABER received the B.Sc. and M.Sc. degrees in computer science from the University of Nantes, France, in 2011 and 2013, respectively, and the Ph.D. degree in computer science from University College Dublin (UCD), Ireland, in 2017. He was a Lecturer/an Assistant Professor with the School of Computer Science, UCD, and the School of Computing, Dublin City University (DCU). He is currently with the School of Computer Science, University of Galway, Galway, Ireland, as a Lecturer/an Assistant Professor. He is also a Post-Doctoral Researcher with the Natural Computing Research and Applications Group, Michael Smurfit Graduate Business School, UCD. He is also a Funded-Investigator in Lero, the Science Foundation Ireland Research Centre for Software. His area of expertise is in the optimization of complex software systems, distributed systems, and wireless communication networks.

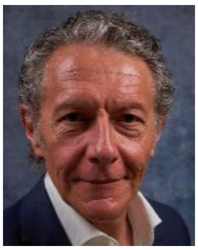

ERNESTO LIMITI (Senior Member, IEEE) has been a Full Professor of electronics with the Electronics Engineering Department, University of Roma “Tor Vergata,” since 2002, after being a Research and Teaching Assistant in 1991 and an Associate Professor in 1998. He is currently the Director of the Microwave Engineering Centre for Space Applications (MECSA), an inter-university center grouping more than 140 researchers in 14 Italian universities. His research activity is focused on modeling for active and passive devices, such as GaAs, GaN, SiC, Si, InP and Diamond MESFET/HEMT, design methodologies for low noise devices/circuits, and linear and nonlinear microwave circuits, including their multi-functional integration (single- chip front-ends, core chips). The above research lines have produced more than 500 contributions on refereed international journals and presentations within international conferences.